

# REENTRY TRAJECTORY DESIGN FOR DEFORMABLE HYPERSONIC VEHICLES BASED ON NEURAL NETWORKS

Chuan-kai Zhou1, Zong-fu Luo\* 1 & Tao Zhang1

<sup>1</sup>School of Systems Science and Engineering, Sun Yat-sen University, 510275 Guangzhou, China

#### **Abstract**

This research explores the application of neural networks to optimize reentry trajectories for deformable hypersonic aircraft, leveraging the advantages of flexible skin technology. By employing a Class Shape Transformation (CST) method for morphing modeling and utilizing the Gauss Pseudospectral Method (GPM) for optimal control problem solving, the paper presents a novel framework. The multilayer feedforward neural network is trained to simulate complex control mappings, reducing online computational demands. The study's simulation experiments highlight the potential of flexible skin in specific mission scenarios and showcase the neural network's robustness in various flight conditions, offering a generalized solution for hypersonic morphing aircraft trajectory optimization.

**Keywords:** Morphing Aircraft, Neural Networks, Reentry Trajectory Optimization, Flexible Skin Technology, Gauss Pseudospectral Method

#### 1. Introduction

Flexible skin is considered one of the future trends in the development of morphing aircraft[1][2]. Compared to rigid deformation techniques with complex structures, high weight, and poor maneuverability[3], deformable wings using flexible skin offer higher performance and a greater flight range[4]. However, the current discussions on flexible skin deformation are primarily focused on wings, with limited exploration of applying flexible skin to lifting bodies. Additionally, although numerical optimal control methods are the main approach for solving optimal control problems, and their stability and computational speed are continuously improving, these methods often have large computational complexity[5]. Thus traditional numerical optimization techniques are still too time-consuming for in online control, such as reentry optimization for hypersonic aircraft under certain disturbances[6]. Meanwhile, the powerful nonlinear mapping capability of neural networks makes them suitable for approximating complex computational models[7], naturally making them suitable for solving a series of nonlinear problems in guidance and control design. By transferring the computational burden to the offline training process, neural networks can reduce the online computational load and shorten the decision-making time for online control.

The first part of this paper focuses on the modeling and traditional method solution for reentry trajectory optimization of a deformable lifting body with flexible skin. Firstly, a parameterized equation based on the Class Shape Transformation (CST) method [8],[9],[10]is used to describe the shape parameters of the deformable lifting body. The Width of fuselage, the shape functions of the upper and lower surfaces, as well as the upper and lower cone angles, can be adjusted using corresponding parameters. The aerodynamic parameters under different shapes are obtained through computational fluid dynamics (CFD) software and interpolated to obtain continuous numerical solutions. Secondly, an optimization model[11] for reentry trajectory is established by extending various deformation variables as control variables. A series of optimal control problems are proposed based on this model to obtain the flight envelope of the deformable lifting body. The control variables for these problems are consistent and include the five deformation parameters mentioned above, as well as bank angle

and attack angle. Subsequently, the Gauss Pseudo method (GPM)[12] is used to solve the relevant optimal control problems in this paper, transforming them into nonlinear programming problems[13]. The optimization indicators for the optimal control problems include maximum lateral range, reachable coverage area, maximum terminal velocity, and minimum flight time, which are compared with the optimization results of the lifting body in the non-deformed state.

The second part of this paper focuses on how to use a multilayer feedforward neural network to simulate the trajectory calculation model and generate control signals[14], reducing the computational burden on onboard devices. Considering that in reality, local conditions or deformation deviations often interfere with the actual flight trajectory, we design a set of scenarios to generate training and testing samples. By introducing deviations to the conditional parameters of the optimal control problems and solving these problems using the GPM to generate numerical solutions for optimal trajectories, which serve as training and testing samples. Numerical simulation experiments are conducted to demonstrate the efficiency and robustness of the proposed methods.

# 2. Aircraft Morphing Modeling and Aerodynamic Parameter Acquisition

# 2.1 Aircraft Generation Based on CST

In the field of aircraft morphing modeling, the Class Shape Transformation (CST) method is favored for its parametric flexibility and efficiency. This study employs the CST method for parameterized modeling of the aircraft to achieve precise control and design of the aircraft's shape. By defining a set of basis functions, the CST method can describe the complex geometric shapes of the lifting body, including both the upper and lower surfaces. These basis functions are adjusted through control parameters to accommodate various flight conditions and performance requirements. This section will detail the process of CST parameterized modeling and its application in the design of aircraft morphing.

The CST method starts by normalizing the curve and transforming the equation of the curve from the physical coordinate system(x,y) to the parametric coordinate system( $y,\eta$ ). The normalized curve equation consists of three parts: the class function C(y), the shape function S(y), and the thickness function T(y), representing the collective properties, the precise shape, and the thickness variation of the curve, respectively.

The class function  $C(\psi)$  is defined as:

$$C(\psi) = \psi^{N_{c1}} (1 - \psi)^{N_{c2}},\tag{1}$$

where  $N_{c1}$  and  $N_{c2}$  are the exponents of the class function, defining the category of the geometric shape.

The shape function  $S(\psi)$  is given by the Bernstein polynomial:

$$S(\psi) = \sum_{i=0}^{n} A_i K_n^i \psi^i (1 - \psi)^{n-i}, \quad K_n^i = \frac{n!}{i!(n-i)!}$$
 (2)

where  $A_i$  and n is are the coefficients and the order of the polynomial, respectively.

The thickness function  $T(\psi)$  is defined as:

$$T(\psi) = \psi t \tag{3}$$

in which t is a fixed parameter.

Integrating the above functions, the CST curve equation can be expressed as:

$$\eta(\psi) = \psi^{N_{c1}} (1 - \psi)^{N_{c2}} \cdot \sum_{i=0}^{n} A_i \frac{n!}{i!(n-i)!} \psi^i (1 - \psi)^{n-i} + \psi t$$
(4)

The aircraft's coordinate system is used as the baseline for parametric modeling, with the Ox axis pointing towards the aircraft's longitudinal axis, the Oz axis within the main symmetry plane of the aircraft and coinciding with the width direction, and the Oy axis perpendicular to the aircraft's main symmetry plane. The length of the aircraft fuselage is denoted as L, with the x-coordinate ranging

from [0,L]; the maximum width is W, with the y-coordinate ranging from [W/2,W/2]. The tail section heights are designated as the lower surface  $H_l$  and the upper surface  $H_u$ , with the z-coordinate ranging from  $[H_l,H_u]$  after simplification. For normalization, we apply the following transformations:

$$\psi == y/W + 0.5 \quad \eta = z/H \tag{5}$$

In the research work of this article, to simplify the problem and focus on the main factors influencing it, we choose to treat the shape function  $S(\psi)$  and the thickness function  $T(\psi)$ . Specifically, we set the coefficients n,t both to 0. This setting means that in this analysis, we are not considering the subtle changes in the airframe curve shape and thickness , in order to more clearly explore the impact of other parameters on the morphing modeling of the aircraft. Thus, the parametric equation for the section curve is expressed as:

$$S(\psi) = 4^{N_{ci}}, i = u, l$$
 (6)

$$C(\psi) = \psi^{N_{ci}} (1 - \psi)^{N_{ci}}, i = u, l$$
(7)

with subscripts u and l representing the upper and lower curves,  $N_{cu}$ ,  $N_{cl}$  representing the exponents of the class function, respectively.

Transforming the parametric coordinates back to physical coordinates, we obtain:

$$z_u = H_u(y/W + 0.5)^{N_{cu}}(0.5 - y/W)^{N_{cu}} \cdot 4^{N_{Cu}}$$
(8)

$$z_l = H_l(y/W + 0.5)^{N_{cl}} (0.5 - y/W)^{N_{cl}} \cdot 4^{N_{C_l}}$$
(9)

$$H_u = tan\theta_u \cdot L \tag{10}$$

$$H_l = tan\theta_l \cdot L \tag{11}$$

$$W = W_{max} \cdot (\frac{x}{L})^{0.5} \tag{12}$$

where  $\theta_u, \theta_l$  is the measure of the upper and lower cone angle.

With all other parameters held constant, the cross-sectional shape of the aircraft can be altered by varying  $W_{max}$ ,  $\theta_u$ ,  $\theta_l$ ,  $N_{cu}$ ,  $N_{cl}$ . These five parameters will also serve as the deformation quantities for further analysis in the subsequent study.

- 1.  $W_{max}$  represents the maximum width of the aircraft's cross-section, which is a fundamental dimension affecting the overall shape and hydrodynamics.
- 2.  $\theta_u$ ,  $\theta_l$  denote the upper and lower cone angles, respectively. These angles influence the curvature and the aerodynamic characteristics of the upper and lower surfaces of the aircraft's tail section.
- 3.  $N_{cu}$ ,  $N_{cl}$  are the bending parameters for the upper and lower surfaces. They determine the degree of curvature or the 'bend' of the surfaces, which can be optimized for various aerodynamic effects.

By considering these parameters as variables, while treating the rest of the parameters as fixed, we can isolate the impact of these deformation quantities on the aircraft's performance. This approach allows for a focused analysis and optimization of the morphing behavior of the aircraft.

# 2.2 Aircraft Morphing Model

A morphing aircraft's ability to transition between various values of deformation parameters is pivotal for adapting to different flight conditions. To facilitate the description and analysis of these transitions with an eye towards expandability, we normalize the maximum width  $W_{max}$ , the upper cone angle  $\theta_u$ , and the upper surface bending parameter  $N_{cu}$  into the deformation variables  $\xi_1, \xi_2$ , and  $\xi_3$ , respectively. The use of normalized variables to represent control quantities is a deliberate choice, allowing for a generalization of our approach beyond the specific deformation quantities discussed. By employing this method, any arbitrary shape parameter can be adapted to the framework of this study, without being limited to the three variables previously mentioned.

The normalized deformation variables  $\xi_i(i=1,)$  are introduced to represent the extent of deformation in a dimensionless manner. This approach not only simplifies the modeling process and allows for a more straightforward application of optimization techniques in the trajectory planning phase but also obscures the specific meaning of the deformation quantities in expression and subsequent calculations. This abstraction enables a broader application of our research methodology to various morphing parameters, enhancing the versatility and adaptability of our trajectory planning framework. For the sake of research convenience and to focus on the most significant effects, this paper models only the extreme values within the deformation range for each variable. By considering only the minimum and maximum values, we create a binary representation of the deformation state, which results in  $2^3$  distinct combinations of deformation states.

We define the deformation variables such that  $\xi_i = 0$  (i = 1, 2, 3) corresponds to the minimum value of the deformation parameter, representing the most conservative or baseline configuration of the aircraft. Conversely,  $\xi_i = 1$  (i = 1, 2, 3) corresponds to the maximum value, indicating the most aggressive deformation state that the aircraft can achieve within the design limits.

The choice of these specific deformation parameters and their normalization is motivated by the desire to construct a trajectory planning problem that can be generalized to various mission profiles and flight conditions. By examining the aircraft's performance across this spectrum of deformation states, we aim to identify optimal trajectories that maximize performance objectives such as range, speed, or efficiency, subject to the constraints imposed by the aircraft's dynamics and the mission requirements.

# 2.3 Aerodynamic Model

This section outlines the process by which we obtain aerodynamic parameter calculations for various angles of attack and Mach numbers following the morphing model establishment. Initially, we present the fitting formulas for the lift coefficient  $C_L$  and drag coefficient  $C_D$  that are pivotal for characterizing the aerodynamic forces acting on the aircraft at different configurations.

The fitting formulas for the aerodynamic coefficients are depicted in the provided figure, illustrating the relationship between the coefficients and the attack angle  $\alpha$  and Mach number Ma. The formulas are as follows:

$$C_L = P_0 + P_1 \alpha + P_2 \alpha^2 + P_3 M a + P_4 M a^2 + P_5 \alpha M a$$
 (13)

$$C_D = Q_0 + Q_1 \alpha + Q_2 \alpha^2 + Q_3 M a + Q_4 M a^2 + Q_5 \alpha M a$$
 (14)

In these equations,  $P_0$  to  $P_5$  and  $Q_0$  to  $Q_5$  are the constant parameters of the lift and drag coefficient expressions, respectively. The attack angle  $\alpha$  and Mach number Ma are the primary variables that influence the aerodynamic performance of the aircraft.

To accurately determine these constant parameters, we apply the least squares method to a carefully selected set of samples. These samples represent the extreme cases where the deformation variables  $\xi_i$  are either at their minimum (0) or maximum (1) values, corresponding to the morphing states with the least and most aggressive deformation, respectively.

For scenarios where the deformation variables take on intermediate values during actual simulations, we utilize linear interpolation to estimate the corresponding aerodynamic coefficients. This method ensures a smooth and accurate representation of the aerodynamics across the full spectrum of deformation states.

The inclusion of the fitting formulas and the corresponding figure provides a visual and mathematical representation of the aerodynamic model, reinforcing the scientific basis of our approach and offering a clear framework for the subsequent trajectory optimization and control algorithm development.

# 3. Reentry Trajectory Design Based on Neural Network

# 3.1 Optimal Control Problem

# 3.1.1 Reentry Dynamic

Considering the relatively short duration of the reentry flight of the aircraft, the influence of the Earth's rotation can be neglected. It is assumed that the Earth is a uniform sphere and the aircraft is a point

mass in unpowered flight. Under the inertial launch coordinate system, the three-degree-of-freedom motion equations of the aircraft can be represented as follows:

$$\begin{cases} \dot{r} = V \sin \theta \\ \dot{\lambda} = \frac{V \cos \theta \sin \psi}{r \cos \phi} \\ \dot{\phi} = \frac{V \cos \theta \cos \psi}{r} \\ \dot{V} = -D - \frac{\sin \theta}{r^2} \\ \dot{\theta} = \frac{1}{V} \left[ L \cos \sigma + \left( V^2 - \frac{1}{r} \right) \frac{\cos \theta}{r} \right] \\ \dot{\psi} = \frac{1}{V} \left( \frac{L \sin \sigma}{\cos \theta} + \frac{V^2}{r} \cos \theta \sin \psi \tan \phi \right) \end{cases}$$

$$(15)$$

where r represents the dimensionless geocentric distance, $\gamma$  and  $\phi$  are the longitude and latitude of the Earth,  $\theta$  and  $\phi$  are the flight path angle and the heading angle, V is the dimensionless velocity,  $\psi$  is the inclination angle. L and D are the dimensionless representations of the lift and drag forces:

$$\begin{cases}
D = \frac{\rho |v|^2 SC_D}{2} \\
L = \frac{\rho |v|^2 SC_L}{2}
\end{cases}$$
(16)

where  $\rho$  is the atmospheric density, S is the reference area,  $C_D$  and  $C_L$  are the drag forces and lift forces.

#### 3.1.2 Path Constraints

To ensure the safety of the aircraft during reentry, the following path constraints should be satisfied:

$$\begin{cases}
q = \rho |v_{rel}|^2 / 2 \leq q_{\text{max}} \\
\dot{Q} = k_Q \sqrt{\rho} |v_{rel}|^3 \leq \dot{Q}_{\text{max}} \\
n_y = |P \sin \alpha + L| / m g_0 \leq n_{\text{ymax}}
\end{cases}$$
(17)

where  $k_Q$  is a coefficient to compute the heating rate and  $g_0$  is the gravitational acceleration at sea level.

# 3.1.3 Scenario Formulation for Reentry Mission

In this study, to demonstrate the versatility and applicability of our approach to reentry trajectory optimization, we have defined three distinct scenarios for the reentry mission of the aircraft. Each scenario is tailored to address specific objectives that are critical for mission success.

#### 1. Maximum Latitude at Target Speed and Altitude

The first scenario is designed to maximize the latitude reached when the aircraft achieves its target speed and altitude . This is particularly important for missions that require precise landing or impact points in high-latitude regions. With  $\gamma_0=0$  and  $\phi_0=0$ , the performance index is set to maximize terminal latitude  $\phi_t$ :

$$J = \min\left[-\phi\left(t_f\right)\right] \tag{18}$$

#### 2. Accessible Area Coverage at Target Speed and Altitude

The second scenario focuses on maximizing the accessible area that the aircraft can cover upon reaching its target speed and altitude. This is crucial for missions that prioritize area reconnaissance or the ability to access a broad range of potential landing zones.

# 3. Maximum Speed at Target Altitude

The third scenario is concerned with achieving the maximum possible speed at the target altitude. This is essential for missions that require rapid reentry to exploit short time windows or for rapid deployment of payloads. The performance index is set to maximize terminal latitude t:

$$J = \min\left[-V\left(t_f\right)\right] \tag{19}$$

By constructing these three scenarios, the primary objective is to explore the performance differences brought about by morphing capabilities from multiple perspectives. This approach allows us to delve into the nuances of how morphing can enhance the reentry trajectory in various mission-critical aspects. Each scenario is meticulously designed to highlight the superior adaptability and performance advantages that aircraft morphing offers, thereby demonstrating the significance of our research.

The scenarios serve as a comprehensive framework to evaluate the impact of morphing on the reentry mission's success. By examining the outcomes across these diverse scenarios, we aim to showcase the robustness and adaptability of the morphing technology. This not only underscores the practical benefits of the aircraft's morphing capabilities but also justifies the innovative approach we have adopted in this study.

# 3.2 Overall Scheme Design

The design of our scheme is anchored in the integration of advanced computational methods and artificial neural networks to facilitate real-time reentry trajectory optimization. The framework is structured into three main components: offline optimal trajectory generation, neural network training, and online control application.

Initially, we employ the Gauss Pseudospectral Method (GPM) to generate a suite of optimal trajectories under various conditions, considering perturbations in aerodynamic coefficients. These trajectories, derived from solving the optimal control problem (OCP) using GPOPS2[15], serve as the foundation for our training samples.

Subsequently, we harness the power of feedforward neural networks to approximate the complex mapping from state variables to control actions. The architecture of our neural network is designed with two hidden layers, utilizing the hyperbolic tangent function as the activation function, ensuring robust performance and generalization capability.

Finally, the trained neural network is evaluated for its ability to replicate the control signals derived from the optimal trajectories. While the current version of the network does not yet meet the precision requirements for real-time online guidance, it demonstrates promising results as a substitute for the control signal sequence solved by the GPM. The control effects produced by the neural network are good, and it exhibits robustness against certain perturbations, indicating its potential as a guidance tool for future aerospace missions

### 3.3 Neural Network Structure

The neural network employed in this study is a multilayer feedforward architecture, designed to capture the nonlinear dynamics of the aircraft's reentry trajectory optimization. As depicted in , the network consists of an input layer, one or more hidden layers, and an output layer, each playing a pivotal role in the learning process.

The nonlinear mapping capability of the network is derived from the composite mapping of simple nonlinear processing units, represented by individual neuron models[16]. Each neuron in the network possesses a threshold and is connected to a set of input neurons through a connection weight matrix w. The activation function, crucial for introducing nonlinearity into the network, is the hyperbolic tangent function, defined as

$$\tanh(x) = \frac{e^x - e^{-x}}{e^x + e^{-x}} \tag{20}$$

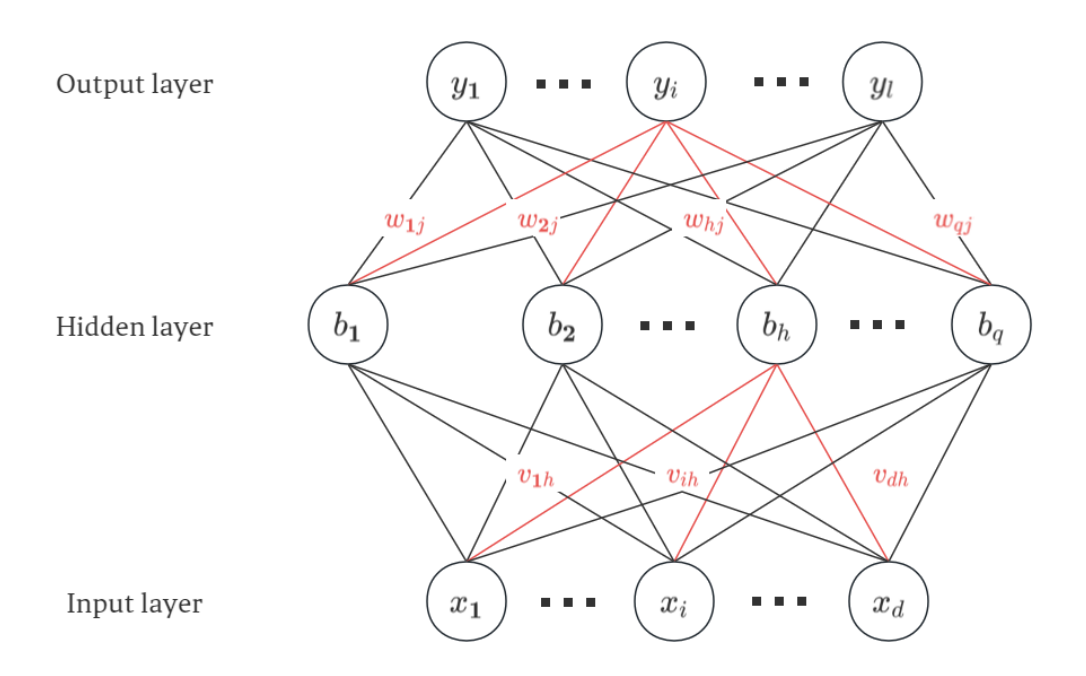


Figure 1 - Three-layer neural network structure

let  $x \in \mathbb{R}^d$  and  $y \in \mathbb{R}^l$  represent the input and output vectors, respectively. The output of the h-th neuron in the hidden layer is denoted as  $b_h$ . The connection weight from the i-th neuron in the input layer to the h neuron in the hidden layer and the connection weight from the h-th neuron in the hidden layer to the j-th neuron in the output layer are represented by  $v_{ih}$  and  $w_{hj}$  respectively. The input of the h-th neuron and j-th neuron are formulated as follows:

$$\alpha_h = f\left(\sum_{i=1}^d v_{ih} x_i\right), \quad \beta_j = \left(\sum_{h=1}^q w_{hj} b_h\right)$$
(21)

For a given training sample  $(x^k, y^k)$ , the network's output is represented by  $\hat{y}^k = (\hat{y}_1^k, \hat{y}_2^k, \dots, \hat{y}_l^k)$ , where each component is computed using the activation function:

$$\hat{y}_{j}^{k} = f(\beta_{j} - \theta_{j}) \quad (j = 1, 2, \dots, l)$$
 (22)

where  $\theta_i$  is the threshold of the *j*-th neuron.

The mean square error for this training sample is expressed as:

$$E^{k} = \frac{1}{2} \sum_{i=1}^{l} \left( \hat{y}_{j}^{k} - y_{j}^{k} \right)^{2}$$
 (23)

The primary requirement of the neural network is to have a strong fitting capability for the training samples. Consequently, the training objective is to minimize the mean square error between the network's predictions and the actual outputs, necessitating the adjustment of all neurons' weight matrices and thresholds. For instance, in the network depicted in 1, there are  $(d+l+1)q \times l$  parameters to be trained, including  $d \times q$  weights from the input to the hidden layer,  $q \times l$  weights from the hidden to the output layer, q thresholds for the hidden layer neurons, and l thresholds for the output layer neurons.

The Error Back Propagation (BP) algorithm is the mainstream method for training multilayer feedforward neural networks. Assuming the training set contains m samples, the BP algorithm optimizes the neural network's parameters by minimizing the accumulated error over the training set

$$E = \frac{1}{m} \sum_{k=1}^{m} E^k \tag{24}$$

The configuration of the neural network for generating control quantities includes six nodes in the input layer, corresponding to the six state variables of the dynamics model. The network comprises two hidden layers with 30 and 15 neurons, respectively, using the hyperbolic tangent function as the activation function. The output layer consists of five nodes, corresponding to the attack angle, the bank angle, and three morphing parameters.

# 3.4 Training and Testing Sample Generation

In our neural network experiments, we have chosen the first scenario designed above to demonstrate the capabilities of our approach. This scenario, which aims to maximize the latitude at the target speed and altitude, provides a comprehensive testbed for evaluating the performance of our neural network under controlled conditions. By focusing on this specific scenario, we can meticulously analyze the network's predictive accuracy and its ability to generate optimal control actions in real-time.

To simulate the dynamic variations in aerodynamic coefficients during flight, we introduce a simplified disturbance model. Assuming uniform atmospheric environmental disturbances, we perturb the lift coefficient  $C_L$  and drag coefficient  $C_D$  according to a Gaussian distribution  $N\left(0,\sigma^2\right)$ , with a 99.5 confidence interval reflecting realistic deviations

$$C_L' = C_L \cdot (1+p) \tag{25}$$

$$C_D' = C_D \cdot (1+q) \tag{26}$$

where p is the deviation coefficient of disturbance to  $C_L$ , and q is the deviation coefficient of disturbance to  $C_D$ ,

Leveraging this model, we generate a comprehensive set of 500 perturbation scenarios. For each scenario, we calculate the corresponding optimal control strategies and state trajectories using GPM, capturing a diverse range of flight conditions. These calculated trajectories form our dataset for training and validating the neural network.

Within the selected scenario, the duration of the flight mission is set between 2000 to 2600 seconds. We have established a sampling interval of 10 seconds to collect pairs of control quantities throughout the entire flight, from initiation to completion. These pairs serve as the inputs and labels for the subsequent training of the neural network.

In this context, 300 sets of perturbation samples are designated for the training dataset, ensuring a diverse and comprehensive range of flight conditions. An additional 200 perturbation samples, coupled with a set of non-perturbed samples, constitute the testing dataset. This partitioning allows for a robust evaluation of the neural network's performance under both typical and atypical flight scenarios.

By following this methodology, we ensure that our neural network is well-equipped to handle the complexities of real-world reentry trajectories, providing a reliable and efficient solution for online trajectory optimization.

# 4. Experimental Results and Analysis

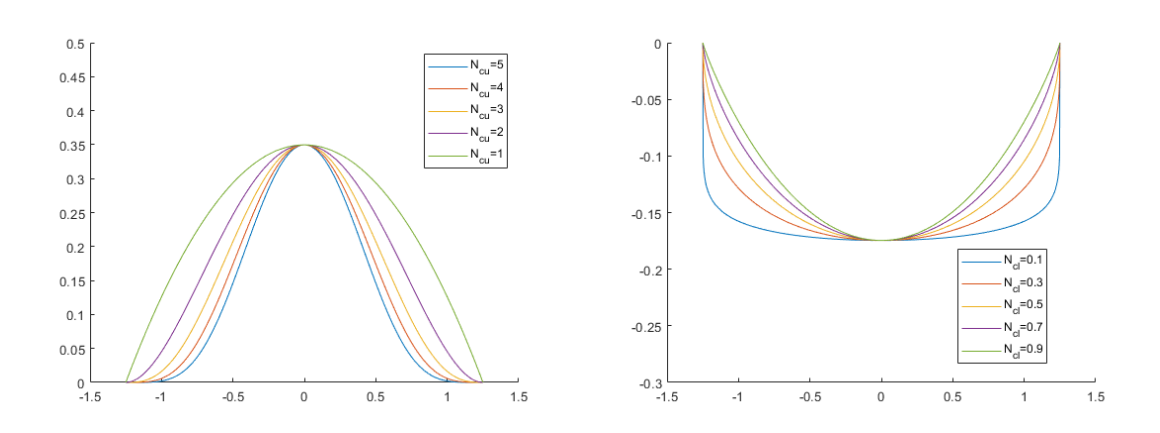
# 4.1 Modeling of the Morphing Aircraft

# 4.1.1 geometric modeling

This section presents the results of the geometric modeling based on the equations 8-12 outlined in Section 2.1. The effects of the parameters  $W_{max}$ ,  $\theta_u$ , and  $\theta_l$ , on the aircraft's shape are quite intuitive and, due to space considerations, are not illustrated with diagrams in this section.

The influence of the parameter  $N_{cu}$  and  $N_{cl}$  on the aircraft's tail section is demonstrated in the following figure 2, which provides a schematic illustration of the tail section.

Simultaneously, using the cross-sectional shape displayed above and by applying the parameters  $\theta_u$  and  $\theta_l$ , the aircraft's fuselage configuration is generated along the main symmetry axis of the aircraft. The resulting conceptual diagram of the aircraft's fuselage is presented in the figure 3.



(a) Variation of Tail Section Curves With different  $N_{cu}$  (b) Variation of Tail Section Curves With different  $N_{cl}$ 

Figure 2 – Influence of Class Function Parameters on Tail Section Curves

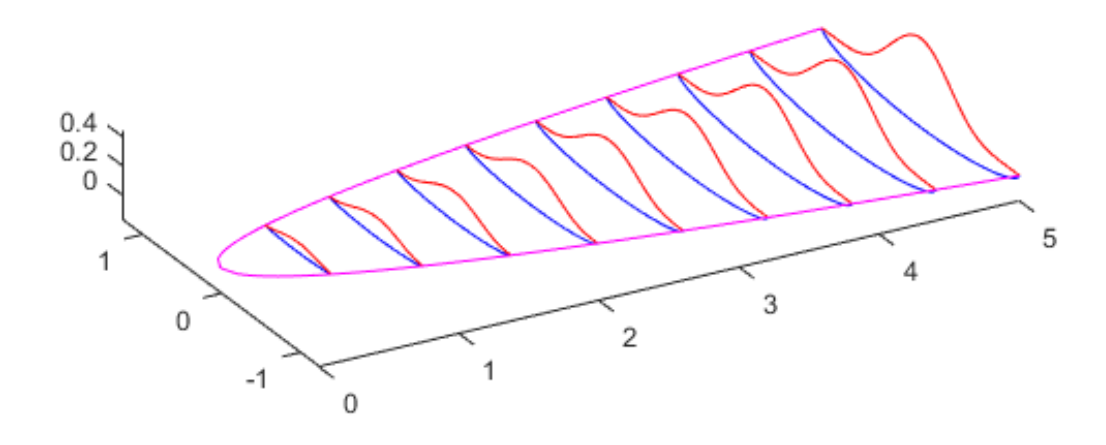


Figure 3 – Conceptual Model of the Lifting Body

# 4.1.2 Aerodynamic Coefficients Comparison Under Different Deformations

The actual modeling was accomplished utilizing the OpenVSP platform, where the WingGeom module was employed to sequentially import airfoil profiles from AF\_Format files of OpenVSP . This process allowed for precise geometric definition and setup of the aircraft model.

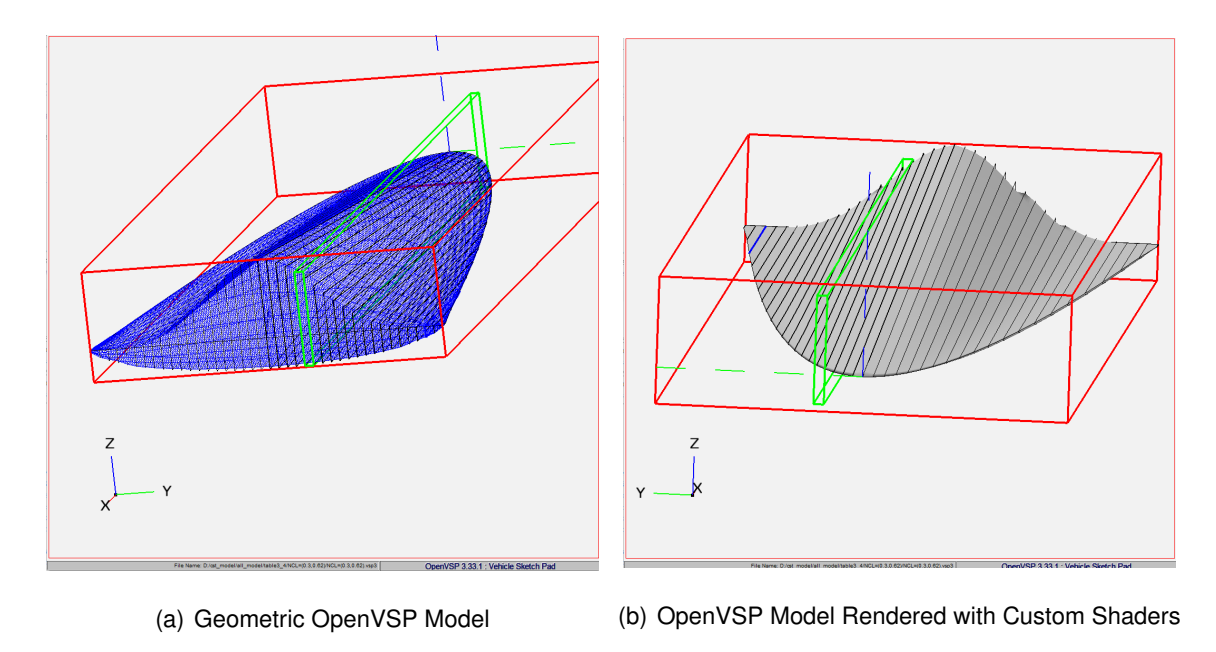


Figure 4 - OpenVSP Model Visualization

For the aerodynamic parameter estimation at Mach numbers ranging from 5 to 15, we utilized the PiFlow as Computational Fluid Dynamics software.

Building upon the aerodynamic data obtained from PiFlow simulations, the least squares fitting method was applied to derive the lift and drag coefficients. The fitting process is depicted in the figure 5.

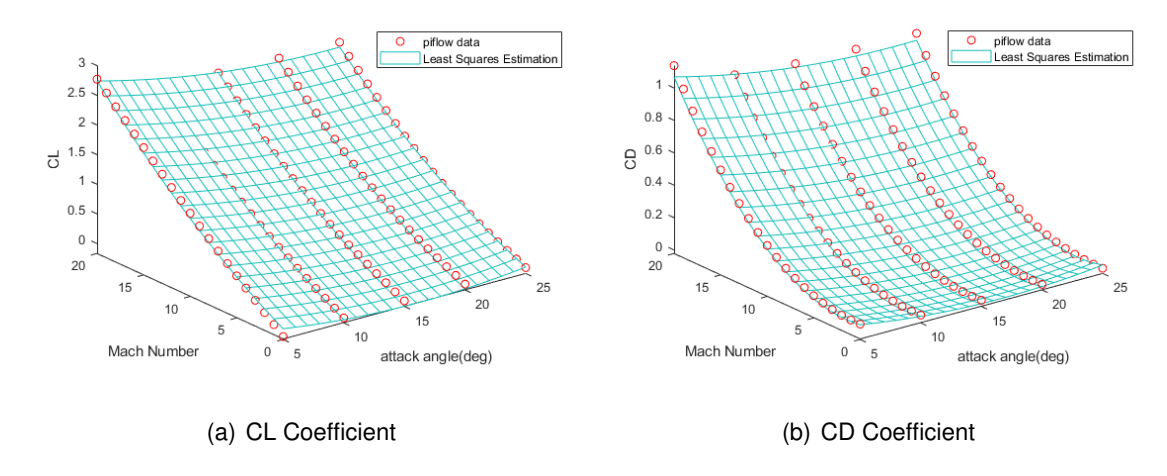


Figure 5 – Aerodynamic Coefficient Surface Derived from Least Squares Estimation

The impact of deformation quantities  $\xi_1, \xi_2$  and  $\xi_3$  on the lift-to-drag ratio is illustrated in the figure 6. With  $\xi_2$  and  $\xi_3$  held constant, the figure demonstrates a "closed region" where the lift-to-drag ratio is favored when  $\xi_1=0$  over when  $\xi_1=1$ . This indicates that there exists a specific range of values for  $\xi_1$  that yields a higher aerodynamic efficiency compared to the extreme value of the parameter. Similar observations can be made for the other two deformation quantities, although for the sake of brevity, these are not elaborated upon here.

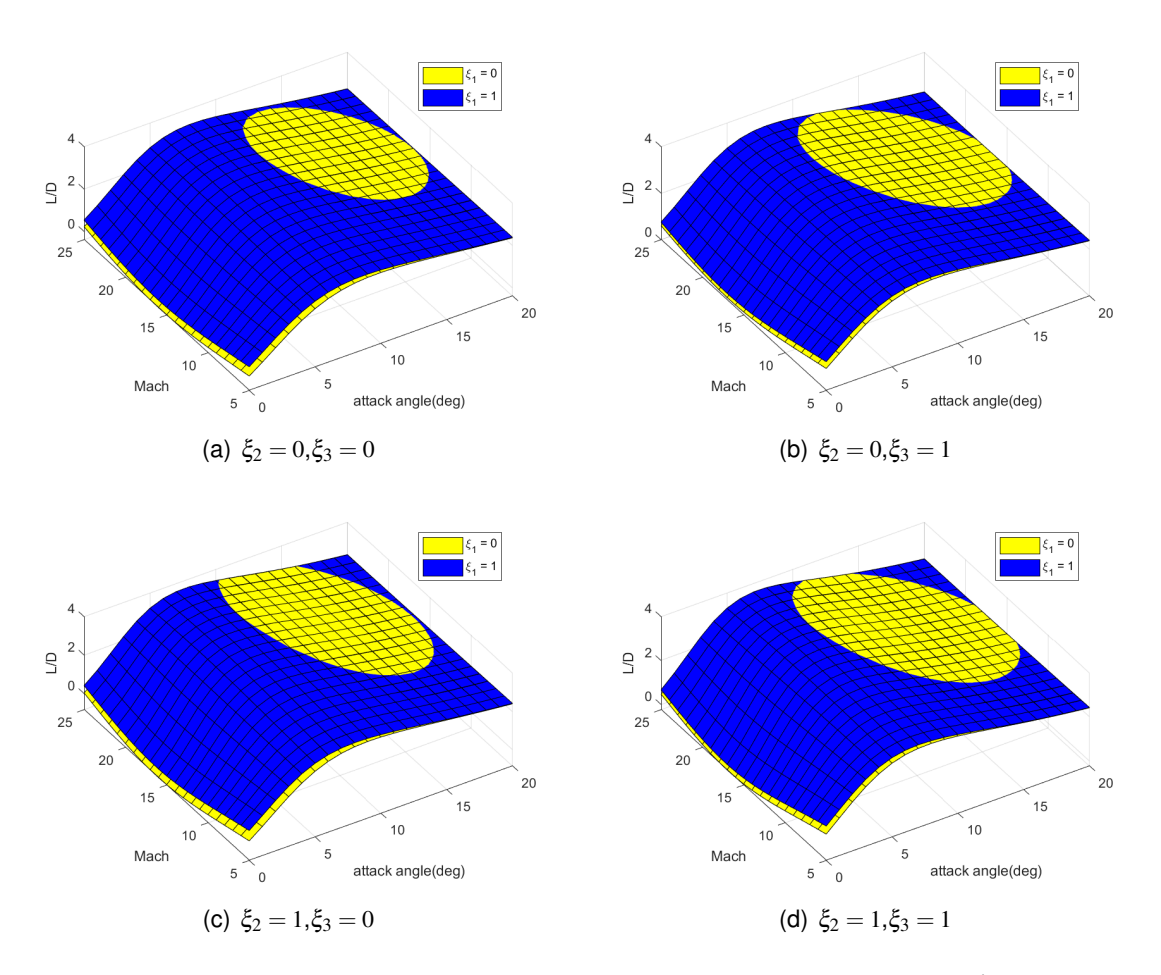


Figure 6 – Comparison of Lift-to-Drag Ratio Surfaces as Deformation Quantity  $\xi_1(N_{cu})$  Changes

Table 1 – Average errors of control-network fitting isolated samples(absolute value)

Category	Training samples	Testing samples	All samples
Average error	1.0745%	1.081%	1.0751%

# 4.2 Optimal Trajectory Solutions

This section presents the optimal trajectory solutions for the reentry mission, leveraging the GPOPS2 software to demonstrate the performance enhancement achievable through the morphing approach introduced in this paper. In Section 3.1.3, "Scenario Formulation for Reentry Mission," three distinct scenarios were formulated to showcase the benefits of the morphing technique for aircraft reentry trajectories.

For the fixed-geometry aircraft, the deformation variables  $\xi_1, \xi_2$ , and  $\xi_3$ , are all set to zero, representing a conventional non-morphing configuration. The following figures 7 illustrate a comparative performance analysis between the Morphing Vehicle and the Fixed Vehicle across the three scenarios.

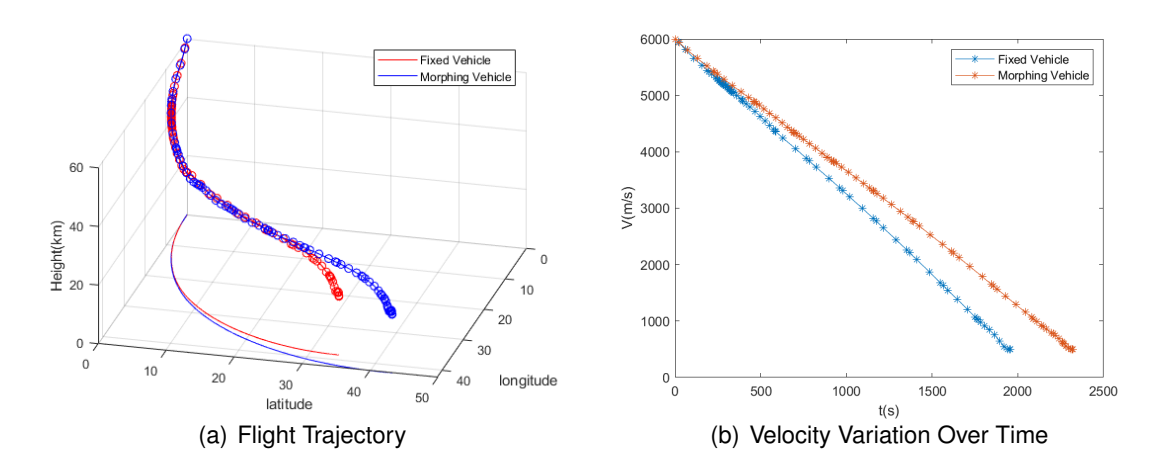


Figure 7 - Maximum Cross-Range Scenario Comparison

The results are compelling: the Morphing Vehicle exhibits an approximate 28% enhancement in maximum cross-range, a 34% increase in the area of the accessible zone, and a 25% improvement in maximum terminal velocity compared to the Fixed Vehicle. These improvements underscore the significant advantages offered by the morphing capabilities of the aircraft, highlighting the potential for optimized mission outcomes.

# 4.3 Neural Network Training and Robustness Testing

In accordance with the procedures outlined in Section 3.4, a dataset comprising 500 trajectory samples has been generated, as depicted in Figure 10. These samples serve as the foundation for training our control network, which is designed to approximate the control signals required for optimal trajectory tracking.

Table 1 presents the average fitting error of the control-network for the samples, providing an initial assessment of the network's performance in replicating the control signals derived from the optimal trajectories. To validate the effectiveness of the control signals produced by the control network, we initiate the integration from the initial state of Scenario One using the optimal trajectory's state variables under nominal conditions as the network input. The integration is performed using the fourth-order Runge-Kutta method (RK4) with a step size of 1 second, and the resulting flight trajectory is illustrated in Figure 11.

It is observed that due to the sensitivity of the attack angle during long-distance hypersonic flight, the integrated trajectory exhibits oscillatory deviations from the optimal trajectory, resembling a wave-like fluctuation. Nonetheless, the terminal state of this integrated trajectory deviates minimally from the nominal trajectory, thereby demonstrating the efficacy of the control signals generated by the network.

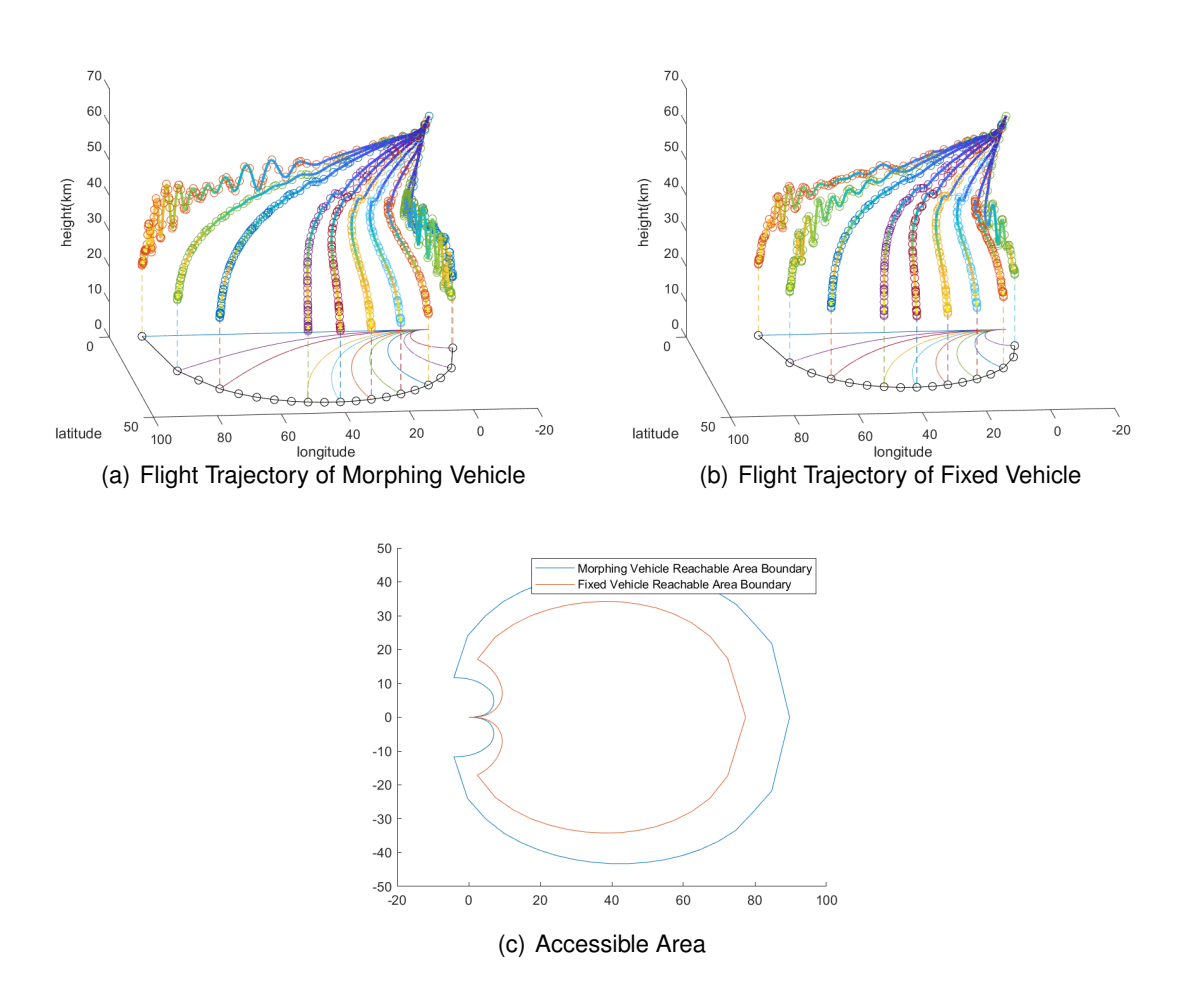


Figure 8 – Accessible Area Comparison

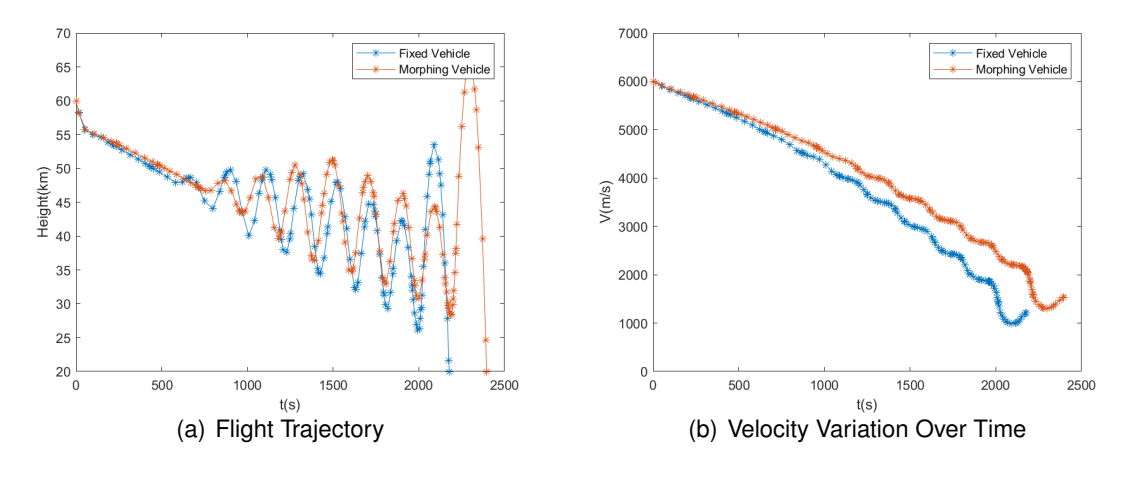


Figure 9 – Max Terminal Velocity Performance Comparison

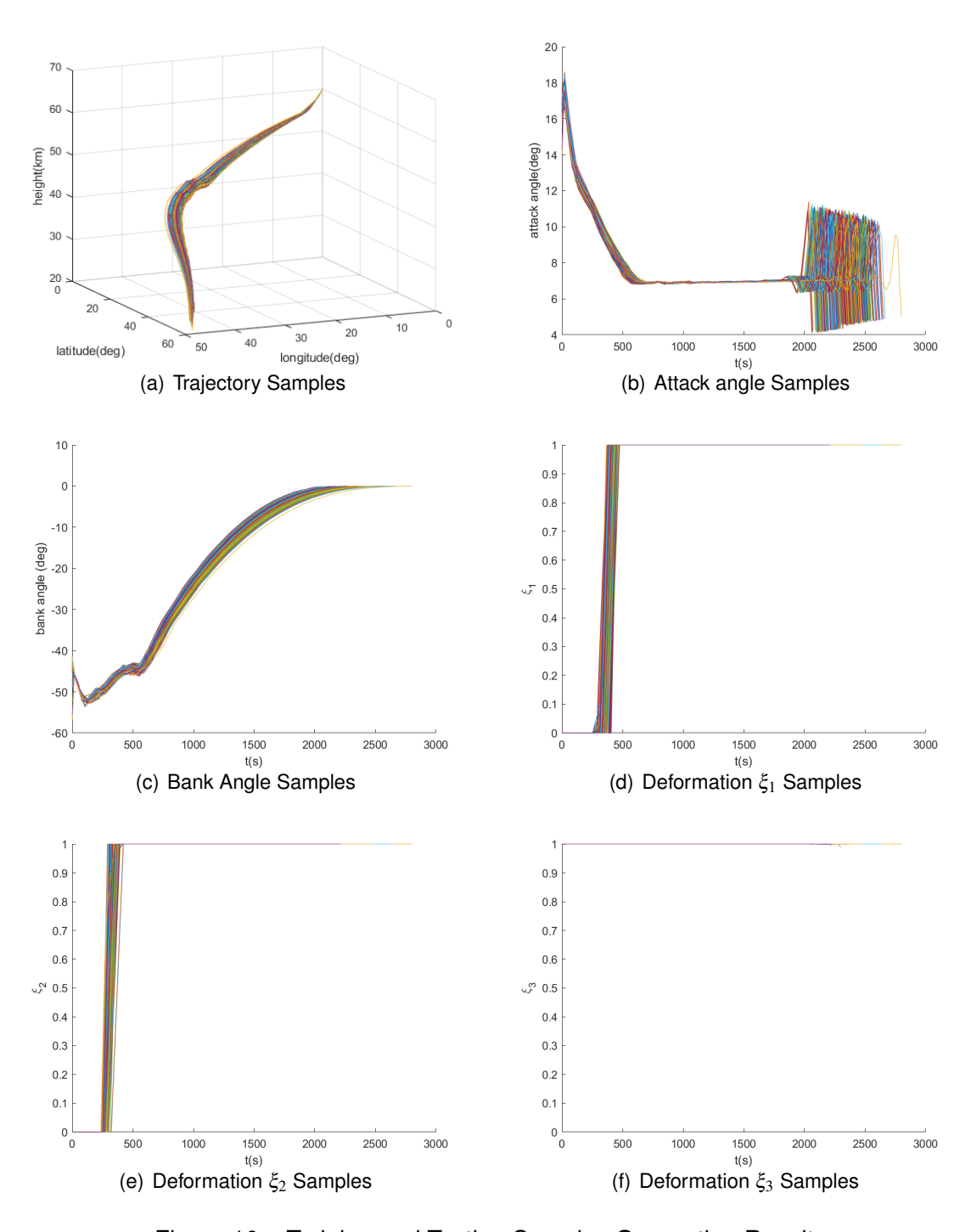


Figure 10 - Training and Testing Samples Generation Results

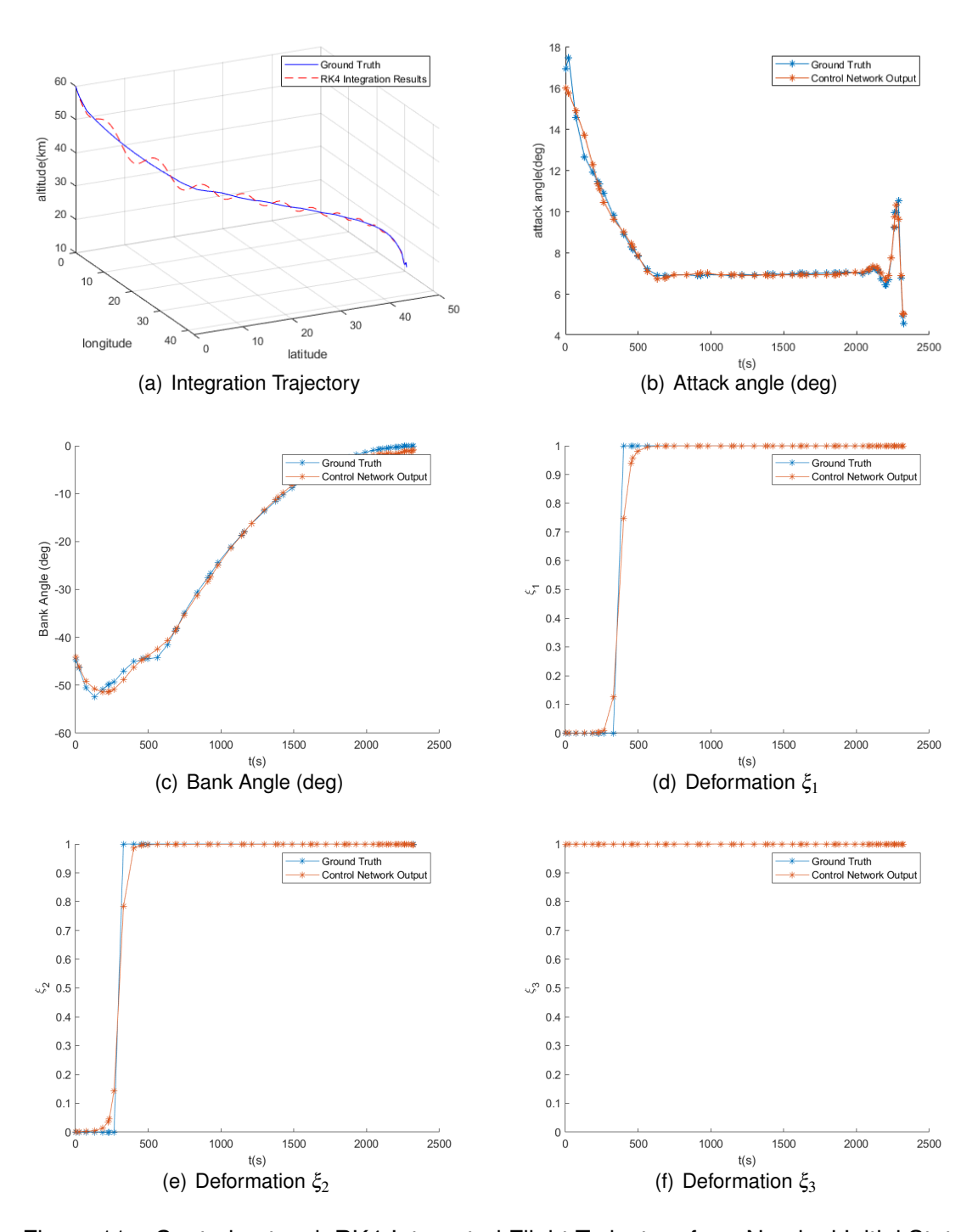


Figure 11 - Control network RK4-Integrated Flight Trajectory from Nominal Initial State

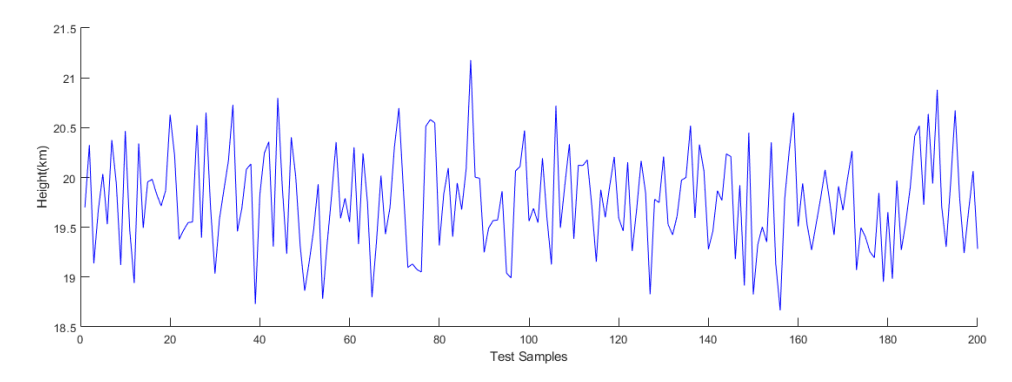


Figure 12 – Terminal heights under 201 sets of test samples

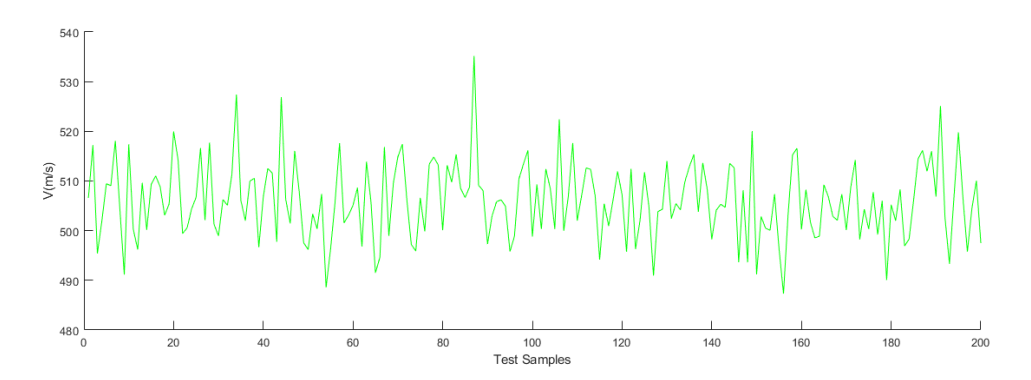


Figure 13 – Terminal Velocity under 201 sets of test samples

Furthermore, to supplement our validation, all samples in the test set have undergone the aforementioned integration process. The terminal altitude of each sample's integrated trajectory is presented in Figure 12, and the terminal velocity is shown in Figure 13. The small margin of error across all test samples underscores the robustness of the network's fitting, indicating its reliable performance even when subjected to a variety of flight conditions.

# 5. Conclusion

This paper presents a comprehensive study on the reentry trajectory design for deformable hypersonic vehicles, showcasing the integration of advanced computational methods and neural networks. Our primary contributions are twofold:

Firstly, we extend the application of flexible skin technology beyond wings to the entire lifting body, providing a detailed analysis of the wing-body integration under various deformation modes. Through simulation experiments, we demonstrate the distinct advantages of lifting bodies with flexible skin deformation in specific mission scenarios, highlighting the potential for enhanced performance and adaptability in flight.

Secondly, we propose a customized approach for training neural networks to simulate control signals under multiple deformation parameters. The offline training and online application of these networks offer a novel solution to the computational challenges associated with real-time trajectory optimization. Our results indicate that the neural network can effectively approximate the complex mappings required for optimal control, exhibiting robustness against perturbations and laying the groundwork for future aerospace applications.

The innovative trajectory planning framework presented in this study not only underscores the practical benefits of morphing aircraft technology but also paves the way for further research and development in the field of aerospace engineering. By examining the aircraft's performance across a spectrum of deformation states, we have identified optimal trajectories that maximize key performance objectives such as range, speed, and efficiency, subject to mission-specific constraints.

In conclusion, our work justifies the adoption of an integrated approach that combines the flexibility of morphing design with the precision of neural network-based control. This research serves as a

testament to the potential of such an approach in advancing the capabilities of hypersonic vehicles and their mission planning.

### 6. Contact Author Email Address

luozf@mail.sysu.edu.cn

# 7. Copyright Statement

The authors confirm that they, and/or their company or organization, hold copyright on all of the original material included in this paper. The authors also confirm that they have obtained permission, from the copyright holder of any third party material included in this paper, to publish it as part of their paper. The authors confirm that they give permission, or have obtained permission from the copyright holder of this paper, for the publication and distribution of this paper as part of the ICAS proceedings or as individual off-prints from the proceedings.

#### References

- [1] James J Joo, Gregory W Reich, and James T Westfall. Flexible skin development for morphing aircraft applications via topology optimization. *Journal of Intelligent Material Systems and Structures*, 20(16):1969–1985, 2009.
- [2] Sara La, W Yeol Joe, Muhammad Akbar, and Bashir Alsaidi. Surveys on skin design for morphing wing aircraft: Status and challenges. In *2018 AIAA aerospace sciences meeting*, page 0315, 2018.
- [3] Bin Zhang, Zhiwei Feng, Boting Xu, and Tao Yang. Free form deformation method applied to modeling and design of hypersonic glide vehicles. *IEEE Access*, 7:61400–61413, 2019.
- [4] Lili Wang, Joshua A Jackman, Ee-Lin Tan, Jae Hyeon Park, Michael G Potroz, Ee Taek Hwang, and Nam-Joon Cho. High-performance, flexible electronic skin sensor incorporating natural microcapsule actuators. *Nano Energy*, 36:38–45, 2017.
- [5] Dario Izzo and Manuel López-Ibáñez. Optimization challenges at the european space agency. In *Proceedings of the Companion Conference on Genetic and Evolutionary Computation*, pages 1399–1415, 2023.
- [6] Jiang Zhao and Rui Zhou. Reentry trajectory optimization for hypersonic vehicle satisfying complex constraints. *Chinese Journal of Aeronautics*, 26(6):1544–1553, 2013.
- [7] Oludare Isaac Abiodun, Aman Jantan, Abiodun Esther Omolara, Kemi Victoria Dada, Nachaat AbdElatif Mohamed, and Humaira Arshad. State-of-the-art in artificial neural network applications: A survey. *Heliyon*, 4(11), 2018.
- [8] Brenda Kulfan and John Bussoletti. " fundamental" parameteric geometry representations for aircraft component shapes. In 11th AIAA/ISSMO multidisciplinary analysis and optimization conference, page 6948, 2006.
- [9] Brenda M Kulfan. Universal parametric geometry representation method. *Journal of aircraft*, 45(1):142–158, 2008.
- [10] Brenda M Kulfan. Recent extensions and applications of the 'cst'universal parametric geometry representation method. *The Aeronautical Journal*, 114(1153):157–176, 2010.
- [11] Zuojun Shen and Ping Lu. Onboard generation of three-dimensional constrained entry trajectories. *Journal of Guidance, control, and Dynamics*, 26(1):111–121, 2003.
- [12] David Benson. *A Gauss pseudospectral transcription for optimal control.* PhD thesis, Massachusetts Institute of Technology, 2005.
- [13] John T Betts. *Practical methods for optimal control and estimation using nonlinear programming.* SIAM, 2010.
- [14] Xin Wang, Pei Dai, Xiaoming Cheng, Yunzhao Liu, Jiashan Cui, Lihua Zhang, and Dongzhu Feng. An online generation method of ascent trajectory based on feedforward neural networks. *Aerospace Science* and *Technology*, 128:107739, 2022.
- [15] Michael A. Patterson and Anil V. Rao. Gpops-ii: A matlab software for solving multiple-phase optimal control problems using hp-adaptive gaussian quadrature collocation methods and sparse nonlinear programming. *ACM Trans. Math. Softw.*, 41(1), oct 2014.
- [16] Ethem Alpaydin. Machine learning. MIT press, 2021.